Vacuum Instability and Pair Production in an Optical Setting

F. Dreisow,[1] S. Longhi,[2] S. Nolte,[1] A. Tünnermann,[1] and A. Szameit[1,*]

[1]*Institute of Applied Physics, Friedrich-Schiller-Universität, Max-Wien-Platz 1, 07743 Jena, Germany*

[2]*Dipartimento di Fisica, Politecnico di Milano and Istituto di Fotonica e Nanotecnologie del Consiglio Nazionale delle Ricerche, Piazza Leonardo da Vinci 32, 20133 Milan, Italy*

(Received 2 May 2012; published 12 September 2012)

In the Dirac-sea picture, the physics of pair production and instability of the quantum electrodynamics vacuum in presence of an oscillating electric field resembles the phenomenon of interband transition of light waves in photonic superlattices induced by a geometric curvature. We realize a binary wave guide superlattice with a curved optical axis mimicking dynamical pair production induced by two counterpropagating ultrastrong laser pulses. Our optical analogue enables visualization of formation of electron-positron pair in physical space as splitting of a wave packet, originally representing an electron in the Dirac sea.

DOI: 10.1103/PhysRevLett.109.110401 PACS numbers: 03.65.Pm, 12.20.−m, 42.50.Xa, 42.82.Et

A remarkable prediction of quantum electrodynamics (QED) is the electron-positron (e^+e^-) pair production (PP) due to the instability of the quantum vacuum in an external electric field [1,2]. As first realized by Dirac, a consistent relativistic quantum description of electrons necessarily involves negative energy levels, which—in the Dirac-sea picture—are filled up to the vacuum state. This entails the striking possibility of pulling an electron out of the vacuum by an electromagnetic field, leaving a hole in the Dirac sea which is associated with a positron. There are basically two main mechanisms of PP involving solely electromagnetic fields: the Schwinger mechanism [3], which requires a strong electrostatic field and dynamical PP [4–7], which occurs in the presence of an oscillating field. The Schwinger mechanism can be regarded as a tunneling process through the energy gap separating negative and positive energy states, whereas dynamical PP can be understood as a multiphoton absorption process. The Schwinger mechanism has never been tested experimentally, because the PP rate is extremely small for electrostatic fields realizable in the lab. The possibility to observe dynamic PP using two counterpropagating ultrastrong laser fields has attracted great interest shortly after the invention of the laser. Recent advantages in ultrastrong laser system facilities promise to provide means to explore this phenomenon [8]. However, the observation of purely laser-induced vacuum instability remains, to date, an experimental challenge [9].

Creating tabletop quantum or classical analogues of extreme dynamical regimes or phenomena in matter which are not accessible in an experiment has attracted increasing interest in recent years. In this way important phenomena and physical models that we have learned in textbooks have been visualized in the lab. Examples include quantum or classical simulations of the event horizon [10], Hawking radiation and black holes [11,12], celestial mechanics [13], the Dirac equation, and relativistic Zitterbewegung [14,15] and Klein tunneling [16]. Experimentally-accessible condensed-matter, matter waves, and optical analogues of PP have been recently proposed as well [12,17–19]. Particularly, the possibility of using graphene to test experimentally the Schwinger mechanism has been proposed [17] and whereas it has been suggested that light transport in a photonic superlattice with a geometric bending [20] mimics dynamical PP [18]. Here, we realize engineered wave guide superlattices to create an optical analogue of PP in an oscillating field, thereby providing the first visualization of the kinematic aspects underlying PP.

The exact description of PP in the framework of QED requires rather generally the determination of an effective action for the interacting Dirac and photon fields, which is a challenging task and can be handled for few cases solely [1,21]. However, for an external (classical) electromagnetic field, in which field dynamics and radiative corrections are neglected, the QED description of PP is relatively simple and the first-quantized picture of Dirac sea is basically retrieved [1]. Such a simplified approach is appropriate to model PP in the antinode of two counterpropagating ultrastrong laser beams and has been discussed in Refs. [6,7,22]. For one spatial dimension x the Hamiltonian of the Dirac field in an oscillating background field is given by $\hat{H} = \int dx \hat{\psi}^\dagger(x)\mathcal{H}(t)\hat{\psi}(x)$, with the two-component spinor operator of the Dirac field $\hat{\psi}(x)$, the single-particle Dirac Hamiltonian $\mathcal{H}(t) = -i\hbar c\sigma_x\partial_x - eA_x(t)\sigma_x + \sigma_z mc^2$, the electron mass and charge, m and e, respectively, and the Pauli matrices $\sigma_{x,z}$. The spatially-homogeneous and time-varying potential $\mathbf{A} = (A_x, 0, 0)$ describes the interaction of the electron with an external oscillating (pulsed) electric field $E_x(t) = -(\partial A_x/\partial t)$ in the dipole approximation. According to the general theory (e.g., Chap. 2 in Ref. [1]), the probabilities of particle scattering and pair creation are determined by the coefficients which connect, via a linear canonical transformation, the "in" and "out" creation and annihilation

operators before ($t \to -\infty$) and after ($t \to \infty$) the interaction with the external field. This problem is basically equivalent to the quantum mechanical (single-particle) scattering problem for the Dirac wave equation with the external classical field, which justifies the first-quantization Dirac sea picture of PP. Moreover, for a spatially homogeneous field the canonical momentum is conserved, and the problem reduces to the determination of the transition probability in a multiphoton absorption process for a driven two-level system, which can be solved by standard numerical or approximate (e.g., WKB) methods [6,22]. In our experiment, we mimic the dynamics of the Dirac equation by considering spatial propagation of monochromatic light waves at wavelength λ in a photonic superlattice comprising alternating sequences A and B of high- and low-index optical wave guides [Fig. 1(a)]. Indicating by a_l the amplitudes of the light field trapped in the various waveguides, in the tight-binding approximation discretized light transport in the lattice is described by the coupled-mode equations [18,20]

$$i\frac{da_l}{dt} = -\kappa \exp(-i\Phi)a_{l+1} - \kappa \exp(i\Phi)a_{l-1} + (-1)^l \delta a_l, \tag{1}$$

where: t is the evolution coordinate; κ and 2δ are the coupling rate and propagation constant mismatch, respectively; $\Phi(t) = (2\pi n_s a/\lambda)(dx_0/dt)$ is the phase term introduced by waveguide bending with profile; $x_0(t)$, a is the waveguides spacing, and n_s is the substrate refractive index. For straight wave guides, ($\Phi = 0$), the tight-binding lattice supports two minibands separated by a gap 2δ [see Fig. 1(b)], defined by the dispersion relation [20] $\omega_{\pm}(q) = \pm\sqrt{\delta^2 + 4\kappa^2 \cos^2(qa)}$ for the Bloch-Floquet modes $a_l(t) \sim \exp(iqla - i\omega t)$ of Eq. (1) with $\Phi = 0$. As discussed in Refs. [15,18], these two minibands are analogous to the positive- and negative-energy branches of the Dirac equation near the band edges $q = \pm\pi/(2a)$. The introduction

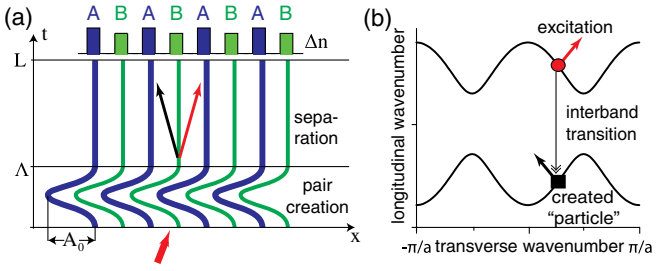

FIG. 1 (color online). (a) Sketch of the geometric arrangement of the wave guide superlattice and corresponding refractive index profile. The arrows indicate excitation and propagation. (b) Band structure of the superlattice. The arrows corresponding to (a) mark the refraction directions in real space. Note that the upper miniband corresponds to the negative-energy (positron) branch of the Dirac field, whereas the lower miniband corresponds to the positive-energy (electron) branch.

of a weak geometric curvature, with $\Phi(t) \to 0$ as $t \to \pm\infty$, induces interband transitions between Bloch modes with the same momentum q belonging to the two different minibands: such a transition precisely mimics the process of dynamic PP induced by a pulsed oscillating field. Let us consider a weak wave guide bending such that $|\Phi| \ll \pi/2$, and excite the array by a broad beam tilted at the Bragg angle, such that Bloch modes with momentum $q \sim \pi/(2a)$ are excited. After setting $a_{2l}(t) = (-1)^l \psi_1(l,t)$, $a_{2l-1} = -i(-1)^l \psi_2(l,t)$, the amplitudes ψ_1 and ψ_2 vary slowly with l, and their evolution is governed by the Dirac equation [18]

$$i\frac{\partial \psi}{\partial t} = -i\kappa\sigma_x \frac{\partial \psi}{\partial l} - 2\kappa\Phi(t)\sigma_x\psi + \delta\sigma_z\psi, \tag{2}$$

where $\psi = (\psi_1, \psi_2)^T$. After the formal change

$$\kappa \to c, \quad \delta \to mc^2/\hbar, \quad l \to x, \quad \Phi \to (eA_x)/(2\hbar c), \tag{3}$$

Eq. (2) corresponds to the one-dimensional Dirac equation $i\hbar\partial_t\psi(t) = \mathcal{H}(t)\psi(t)$. In our optical analogue the *temporal* evolution of the spinor wave function ψ for the Dirac electron is mapped onto the *spatial* evolution of the field amplitudes ψ_1 and ψ_2 along the array, which correspond to the occupation amplitudes in the two sublattices A and B of Fig. 1(a). The local curvature (d^2x_0/dt^2) of the wave guides determines the shape of the pulsed field $E_x(t)$, and can be engineered to simulate PP in the antinode of two counterpropagating, ultrastrong and single-cycle laser pulses. In the Dirac sea framework, a simple picture of PP has been suggested in Ref. [7]. Here an electron in the negative sea is represented by a Gaussian wave packet formed by a superposition of negative-energy states. When the e^+e^- pair is produced after the action of the laser pulses, a droplet is separated from the wave packet and moves opposite to the initial one. The droplet is a positive-energy state and represents the created electron. For a nearly-monochromatic low-amplitude ac field with a frequency $\omega = 2\pi/\Lambda$ much smaller than the frequency gap 2δ, i.e., for an ac field with a photon energy $\hbar\omega$ much smaller that twice the electron rest energy $2mc^2$, the transition of one electron out of the Dirac sea into a positive-energy state generally occurs via a multiphoton process, and a n-photon resonance condition should be satisfied [7]. This is the typical condition attainable with laser-driven QED vacuum, and phenomena like Rabi oscillations of the quantum vacuum have been predicted in this way [6]. For single-cycle high-frequency ac fields with strong amplitudes, the transition of one electron out of the Dirac sea is not a resonance process and the probability P of PP depends on the amplitude, frequency and phase of the pulsed field in a rather complex way [18]. In our photonic experiments, we simulated the process of PP in the latter regime, i.e., using a single-cycle ac pulse, in the extreme (nonperturbative) regime of QED. The optical analogue of PP can be basically viewed as an interband transition of a light

beam in a wave guide superlattice induced by bending, which mimics the action of the single-cycle ac field. The PP is visualized as a breakup of an initial Gaussian wave packet belonging to the (in optical terms) upper Bloch miniband of the superlattice. Wave guide bending induces partial light transfer into the lower miniband of the superlattice, and the two wave packets belonging to the two minibands refract along two opposite directions and separate each other, as schematically shown in Fig. 1(b).

The experimental realization was managed in optical wave guide arrays fabricated via femtosecond laser wave guide writing [23]. The idea of implementing a wave guide array mimicking relativistic quantum mechanics was adapted from previous experiments, where high and low effective indices are achieved by low and high writing velocities [15]. The high-frequency single-cycle ac field is realized by engineering the bending profile $x_0(t)$. The first section of the array is a harmonically curved lattice with the peak-to-peak amplitude A_0 and period Λ, subsequently followed by a straight passage until the end of the sample [Fig. 1(a)]. The wave guide spacing was set to $a = 12$ μm in order to achieve sufficient coupling in the straight section of $\kappa = 0.24$ mm^{-1}. The period of the single-cycle pulse was fixed to $\Lambda = 6.67$ mm in all the samples, whereas two sets of superlattices with small and large detunings ($\delta = 0.4\kappa$ and $\delta = 0.8\kappa$) were investigated, which simulate PP for two different ratios of the photon energy $\hbar\omega$ of the external field to the rest energy mc^2 of the electron. For a fixed ratio δ/ω, the probability P of PP after the pulse is a function of the peak pulse amplitude A_0, and can be numerically computed as discussed in Refs. [6,18]. The length of the samples was $L = 90$ mm. The amplitude A_0 of the modulated section was tuned from 0 to 48 μm in a set of 13 realizations. Light propagation along the samples was visualized via wave guide fluorescence microscopy [24], which provides mapping of the evolution of the wave packet distribution versus t. We excite the wave guide arrays with a negative-energy Gaussian wave packet corresponding to the wave packet of an electron in the Dirac sea; this was accomplished by focusing onto the sample's input facet a laser beam at an incidence angle $\theta = \lambda/(8n_s a)$ (i.e., half the Bragg angle), corresponding to a width of 9 wave guides and a transverse wave number $q = \pi/(4a)$. In this way, the lowest-energy miniband of the array is mostly excited [18]. For vanishing ac field ($A_0 = 0$) the wave packet propagates as a collimated beam to the right hand side undergoing a weak broadening due to discrete diffraction; i.e., no interband transition occurs. As the strength of the ac field A_0 is increased, an interband transition is observed, which can be visualized as a breakup of the initial wave packet into two wave packets that refract into opposite directions and separate during the further propagation. As shown in Fig. 1(b), in the vicinity of the Dirac point the two minibands have different signs in their derivative and therefore the direction of the propagating beams belonging to the two minibands are opposite. The fractional light power carried by the newly created wave packet, propagating in the opposite direction than the initial wave packet, is precisely the probability P of PP. In our experiments, P can be thus simply measured by integrating the light intensity in the left half of the array and normalizing to the total light intensity at $t = L$. For the set of samples corresponding to a small miniband gap of $\delta = 0.4\kappa$, the theoretical model indicates that the probability P of PP is maximum at $A_0 \simeq 28$ μm but only 40% of the incident light is transferred into the positive-energy band. This means that the ratio between photon energy of the ac pulse ($\propto 1/\Lambda$) and the rest energy of the electron ($\propto \delta$) is not appropriately adjusted, resulting in a fractional probability for PP. Examples of the beam evolution are shown in Fig. 2, which depicts the measured light intensity maps and corresponding numerical results as obtained from Eq. (1). Note, that in the experiments a third beam occurs, which is a remainder of the injected laser light not coupled into the wave guides. This beam is not relevant to the physics of the simulated PP process and it is not observed in the numerical simulations, which are based on a discretized (tight-binding) model of light transport. Additionally, the tight binding model (1) is only an approximate model for our experiments as the lattice spacing is rather small ($a = 12$ μm). Therefore, the actual miniband shapes slightly deviate from the tight-binding curves $\omega_{\pm}(q)$ and differ in the upper and lower bands, yielding slightly

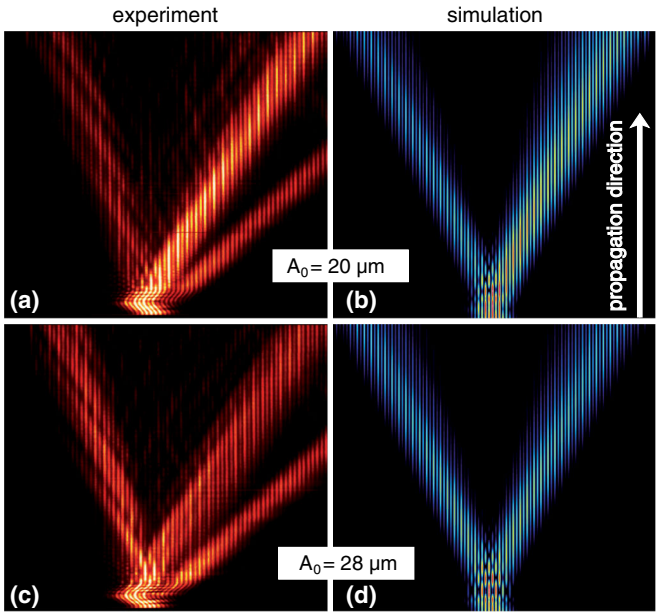

FIG. 2 (color online). Beam propagation images in the wave guide superlattice for $\delta = 0.4\kappa$ and for (a,b) $A_0 = 20$ μm, and (c,d) $A_0 = 28$ μm. For the sake of clearness, the simulated light intensity distributions are plotted in the wave guide reference frame, where the array appears to be straight. The probability for PP (left beam) is only fractional.

different propagation angles of the left and right beams observed in (a) and (c).

To optimize the PP probability P, in a series of numerical simulations we scanned the detuning δ, at the fixed value of the oscillation frequency $\omega = 2\pi/\Lambda$, and found that P can reach a value close to 100% for a miniband gap $\delta = 0.8\kappa$. The numerical simulations shown in Figs. 3(b), 3(d), and 3(f) indicate that the probability P of PP first increases as the amplitude A_0 of the ac field is increased, reaching a maximum at $A_0 \simeq 28$ μm, where the entire light beam is transferred from the negative-energy to the positive-energy miniband. After the curved section of the lattice, the beam then propagates to the left hand side according to the opposite sign in the transverse group velocity. As the ac field amplitude A_0 is further increased, the probability P is reduced. Correspondingly, the wave packet splits again into two beams indicating the occupation of both bands with almost equal probabilities. The corresponding experimental results are shown in Figs. 3(a), 3(c), and 3(e). Figure 3(a) depicts a case with low amplitude $A_0 = 20$ μm, where approximately half of the light has been transferred to the positive-energy band. The sample with $A_0 = 28$ μm realizes an almost complete transition with $P \simeq 95\%$, while in Fig. 3(c) the amplitude of $A_0 = 44$ μm shows again the occupation of both bands.

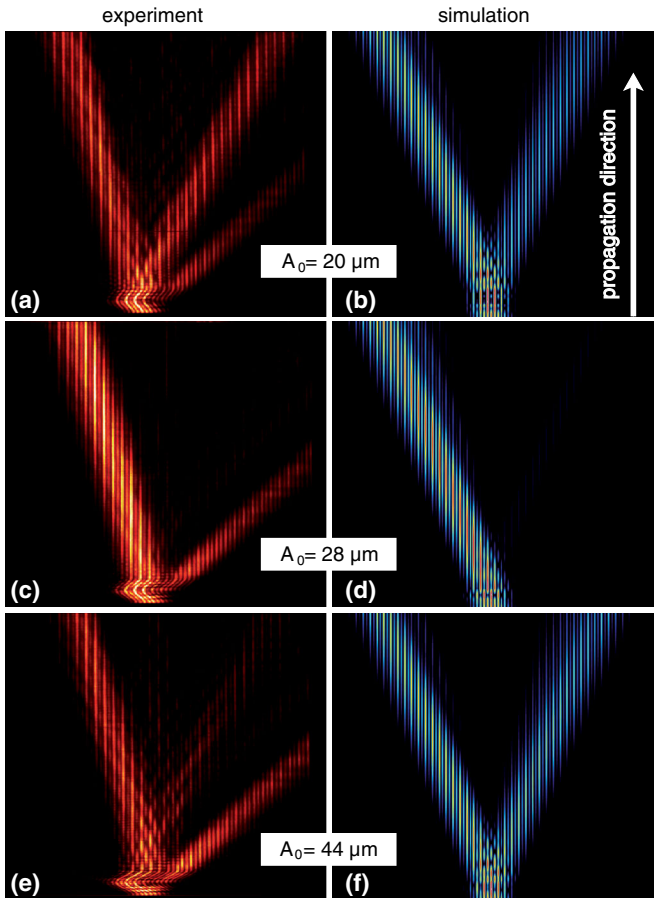

FIG. 3 (color online). Same as Fig. 2 but for a larger detuning $\delta = 0.8\kappa$, corresponding to a smaller ratio of the photon energy to the rest energy of electron. (a,b) $A_0 = 20$ μm, (c, d) $A_0 = 28$ μm, and (e,f) $A_0 = 44$ μm. For an amplitude $A_0 = 28$ μm the probability for pair creation approaches unity.

The detailed behavior of the PP probability P versus the ac-field amplitude A_0, for the two sets of samples corresponding to the small and large miniband gaps, is shown in Fig. 4(a). In the figure, the points (circles/squares) and curves (solid/dashed) refer to the experimental and theoretical results, respectively. Figures 4(b) and 4(c) show the detailed distributions of light intensity at the output plane of the arrays, i.e., at $t = L$, for increasing values of A_0 and for the small [Fig. 4(b)] and large [Fig. 4(c)] miniband gaps. The figures clearly indicate that for vanishing or small values of the amplitude A_0 the light exits the sample at the right hand side (no PP). Beam break up occurs as A_0 is increased, and some light appears in the left hand side of the sample; this fractional light power is precisely the probability P of PP. Figure 4 clearly shows that P is not a monotonically increasing function of the amplitude A_0, and that the PP process for strong and high-frequency fields can not be explained in the framework of a multiphoton resonance process.

In conclusion, we have optically simulated one of the most exciting and older predictions of relativistic QED theory, namely vacuum instability and dynamical PP induced by an oscillating electric field. Our photonic simulator, based on light propagation in a wave guide superlattice, is able to exactly reproduce the kinematic aspects of the PP process in the framework of the Dirac-sea picture. Such results indicate that photonic simulators based on wave guide lattices provide a feasible and accessible test bed to visualize nonperturbative and extreme dynamical

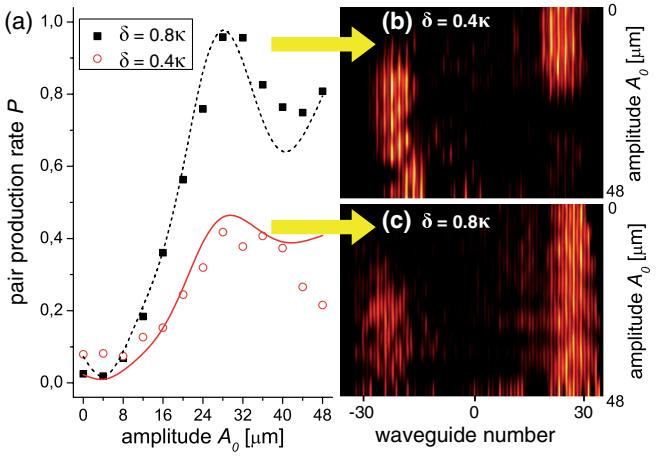

FIG. 4 (color online). (a) Behavior of the PP probability P versus the ac-field amplitude A_0 (theory and experimental data points) for $\delta = 0.4\kappa$ and $\delta = 0.8\kappa$. (b) and (c) show the measured light intensity distributions at the exit of the arrays for increasing values of A_0 and for the two values of detunings δ. In (b) the maximal PP probability is $<50\%$, whereas in (c) the probability approaches unity at $A_0 = 28$ μm.

regimes of QED, which are still out of a direct experimental observation.

We acknowledge support by the MIUR (PRIN 2008 project), BMBF (ZIK 03Z1HN31), DFG (NO462/6-1), TMBWK (FKZ: 11027-514) and Graduate Research School OptiMi (B514-10061).

*Corresponding author: alexander.szameit@uni-jena.de

[1] E. S. Fradkin, D. M. Gitman, and Sh. M. Shvartsman, *Quantum Electrodynamics with Unstable Vacuum* (Springer, Berlin, 1991).
[2] H. K. Avetissian, *Relativistic Nonlinear Electrodynamics* (Springer, New York, 2006).
[3] F. Sauter, Z. Phys. **69**, 742 (1931); W. Heisenberg and H. Euler, Z. Phys. **98**, 714 (1936); J. Schwinger, Phys. Rev. **82**, 664 (1951).
[4] E. Brezin and C. Itzykson, Phys. Rev. D **2**, 1191 (1970).
[5] V. S. Popov, JETP Lett. **18**, 255 (1973); D. B. Blaschke, A. V. Prozorkevich, C. D. Roberts, C. S. M. Schmidt, and S. A. Smolyansky, Phys. Rev. Lett. **96**, 140402 (2006); C. C. Gerry, Q. Su, and R. Grobe, Phys. Rev. A **74**, 044103 (2006).
[6] H. K. Avetissian, A. K. Avetissian, G. F. Mkrtchian, and K. V. Sedrakian, Phys. Rev. E **66**, 016502 (2002); A. Di Piazza, Phys. Rev. D **70**, 053013 (2004).
[7] M. Ruf, G. R. Mocken, C. Muller, K. Z. Hatsagortsyan, and C. H. Keitel, Phys. Rev. Lett. **102**, 080402 (2009).
[8] Y. I. Salamin, S. X. Hu, K. Z. Hatsagortsyan, and C. H. Keitel, Phys. Rep. **427**, 41 (2006); F. Ehlotzky, K. Krajewska, and J. Z. Kaminski, Rep. Prog. Phys. **72**, 046401 (2009).
[9] Experiments have so far demonstrated PP in laser-proton or laser-electron collisions (see Ref. [8] and references therein), but not in purely laser fields.
[10] T. G. Philbin, C. Kuklewicz, S. Robertson, S. Hill, F. Königand, and U. Leonhardt, Science **319**, 1367 (2008).
[11] F. Belgiorno, S. L. Cacciatori, M. Clerici, V. Gorini, G. Ortenzi, L. Rizzi, E. Rubino, V. G. Sala, and D. Faccio, Phys. Rev. Lett. **105**, 203901 (2010); O. Lahav, A. Itah, A. Blumkin, C. Gordon, S. Rinott, A. Zayats, and J. Steinhauer, Phys. Rev. Lett. **105**, 240401 (2010).
[12] R. Schützhold, Adv. Sci. Lett. **2**, 121 (2009).
[13] D. A. Genov, S. Zhang, and X. Zhang, Nature Phys. **5**, 687 (2009).
[14] R. Gerritsma, G. Kirchmair, F. Zähringer, E. Solano, R. Blatt, and C. F. Roos, Nature (London) **463**, 68 (2010).
[15] F. Dreisow, M. Heinrich, R. Keil, A. Tünnermann, S. Nolte, S. Longhi, and A. Szameit, Phys. Rev. Lett. **105**, 143902 (2010).
[16] A. F. Young and P. Kim, Nature Phys. **5**, 222 (2009); R. Gerritsma, B. P. Lanyon, G. Kirchmair, F. Zähringer, C. Hempel, J. Casanova, J. J. García-Ripoll, E. Solano, R. Blatt, and C. F. Roos, Phys. Rev. Lett. **106**, 060503 (2011).
[17] D. Allor, T. D. Cohen, and D. A. McGady, Phys. Rev. D **78**, 096009 (2008).
[18] S. Longhi, Phys. Rev. A **81**, 022118 (2010).
[19] N. Szpak and R. Schützhold, Phys. Rev. A **84**, 050101(R) (2011).
[20] F. Dreisow, A. Szameit, M. Heinrich, T. Pertsch, S. Nolte, and A. Tünnermann, Phys. Rev. Lett. **102**, 076802 (2009).
[21] R. Ruffini, G. Vereshchagin, and S.-S. Xuea, Phys. Rep. **487**, 1 (2010).
[22] S. P. Gavrilov and D. M. Gitman, Phys. Rev. D **53**, 7162 (1996); H. Kleinert, R. Ruffini, and S.-S. Xue, Phys. Rev. D **78**, 025011 (2008); C. K. Dumlu, Phys. Rev. D **79**, 065027 (2009); G. R. Mocken, M. Ruf, C. Muller, and C. H. Keitel, Phys. Rev. A **81**, 022122 (2010); C. K. Dumlu and G. V. Dunne, Phys. Rev. D **83**, 065028 (2011).
[23] K. Itoh, W. Watanabe, S. Nolte, and C. B. Schaffer, MRS Bull. **31**, 620 (2006).
[24] A. Szameit, F. Dreisow, H. Hartung, S. Nolte, A. Tünnermann, and F. Lederer, Appl. Phys. Lett. **90**, 241113 (2007).